ETHANOL TURBULENT SPRAY FLAME SIMULATION WITH RANS

Fernando Luiz Sacomano Filho, fernando.sacomano@gmail.com
Newton Kyoshi Fukumasu, newton.fukumasu@gmail.com
Escola Politécnica da Universidade de São Paulo - Av. Prof. Mello Morais, 2231 - Cidade Universitária – SP - CEP: 05508-030

Guenther Carlos Krieger Filho, guenther@usp.br
Escola Politécnica da Universidade de São Paulo - Av. Prof. Mello Morais, 2231 - Cidade Universitária – SP - CEP: 05508-030

Abstract. *Several industrial devices use combustion spray processes. The main advantage of this process is to improve specific power, which provides compact devices design. Currently, the interest in the utilization of bio fuels is increasing as an alternative to the reduction of carbon dioxide emission, know as one of the chemical substances responsible for the global warming. This work reports a numerical modeling of an ethanol turbulent spray flame. The models employed were compared with experimental data from a study of turbulent spray flame. The model is based on the finite volume method for low Mach number and steady state flow development. The spray was calculated using the Separated Flow method (SF) with an Euler-Lagrange model, where the gaseous phase was described by an Eulerian model and the liquid phase by a Lagrangian particle method. Both phases are coupled in order to account for shared effects. The turbulence model k-ε Standard was used to determine the dispersant phase. Effects related to the turbulence interference into the dispersant phase by the disperse phase were disregarded. Evaporation of droplets was calculated with the assumption of the infinite-liquid-conductivity model, where the droplet inner temperature is uniform, but varies with the mass and heat transfer within the dispersant phase. The combustion modeling was done with the transport of the mixture fraction and the conventional β-PDF flamesheet model. Evaporative cooling by the liquid phase and radioactive heat transfer were not accounted for in this work.Reasonable agrement between measured and computed mean profiles of temperature and velocity was achieved. The deviations observed in the results are attributed to the over predicted diffusion of the mean quantities transported, which produces a displacement between the results from simulations and experiments.*

Keywords*: ethanol, turbulent, spray, flame,combustion*

1. INTRODUCTION

Spray combustion is applied in liquid-fuel gas turbines, internal combustion engines, industrial furnaces, and other engineering devices. Because of convenience in transport, flexibility in storage, availability in liquid phase, a significant portion of the total energy demand has been met by the combustion of liquid fuels injected as spray into the combustion chamber (Kuo, 1986). The physics of this phenomenon is extremely complex (Apte et al., 2009). Usually the liquid fuel is injected into a combustion chamber by an atomization process, allowing a spray to develop. The resulting droplets evaporate and mix with the oxidizer yielding an ignitable mixture. Chrigui *et al.* (2009) enounces the prediction of droplet characteristics such as mean and fluctuating velocities, droplet and vapor distributions, and carrier phase properties are mandatory for improving performance in future engineering devices fired by liquid fuels.

In the present work, emphasis is placed on simulation of evaporating spray in an open ethanol turbulent spray flame. Detailed experimental data and boundary conditions of the analyzed flame were presented by Masri (2009). The approach was based on an Euler-Lagrange method with Reynolds Averaged Navier Stokes simulations for the gaseous phase and Lagrangian equations for the liquid phase.

The predictive capability of the Euler-Lagrange approach for ethanol spray evaporation is evaluated. The assumption of subgrid scale dynamic for the discrete phase is done so that the particle diameter (d_P), its length scale, is assumed smaller than the grid size.

Most numerical investigations of particle-turbulence interactions with large number of particles (on the order of millions) use DNS, LES or RANS for the continuum carrier phase and 'point-particle (PP)' assumption for the dispersed phase (Apte *et al.*, 2009). The procedure of computing each droplet was made to better reproduce the droplets distribution in the flow domain, which is directly dependent of the injection distribution. As Düwel et al. (2007), Rochaya (2007) and Faeth (1983) mention in their respective work the results of the simulations of sprays are very sensitive to droplet injection distributions. Masri (2009) presents an experimental device that allows good specification of boundary conditions, giving well defined inputs to numerical simulations. Thus, the data of Masri (2009) were used here. Fluent (2006) presents that better reproduction of the injection process in simulations is done with stochastic models, thereby the option for a stochastic model was done in this work.

Düwel et al. (2007) have performed two-dimensional axisymmetric k-ε simulations with Standard values for the adjustable constants of non-reacting and reacting ethanol sprays in an open air chamber. For the reacting case, a detailed ethanol/air combustion mechanism has been implemented through a spray flamelet model. The chemical reaction mechanism includes 38 species and 337 elementary reactions. In their work an Eulerian–Lagrangian formulation was applied to calculate the development of both non-reactive and reactive sprays. The simulation results were compared

with experimental data of a liquid spray generated by a pressure atomizer. This kind of atomizer hampers the characterization of droplets distribution, next to the nozzle, and also, the modeling the spray with the Euler-Lagrange method. Next to the nozzle the spray is not dilute. Despite these problems they showed that simulation results were close to experimental data.

Rochaya (2007) have performed tridimensional periodic Reynolds stress simulations of non-reacting and reacting ethanol sprays in an open air chamber and in a pressure varying swirling combustion chamber. For the reacting case, a detailed ethanol/air combustion mechanism was implemented through a conventional β-PDF laminar flamelet model. The chemical reaction mechanism was obtained from Marinov (1999) work, which includes 56 species and 351 elementary reactions. Also, in their work an Eulerian–Lagrangian formulation was applied to calculate the development of both non-reactive and reactive sprays. The liquid spray, which composes his experimental data, is generated by a pressure swirl atomizer. This kind of atomizer generates the same spray dilution characteristics encountered in the work of Düwel et al. (2007). Rochaya (2007) states that the simulations over predict the evaporation rate, and the correlation used to account for the convective effects was believed to be the main cause of the discrepancy. The over predicted evaporation rate led, to an under prediction of the flame temperature in the vicinity of the spray nozzle, where the fuel is too rich to burn – unlike the behavior observed in his experiments. This also resulted in a cooled region due to the passage of the spray that was significantly wider than observed experimentally.

2. MATHEMATICAL MODELING

The mathematical modeling in this work was based on the variable density, low-Mach number equations for the gaseous phase. Any acoustic interactions and compressibility effects were neglected. Despite focusing on steady-state simulation in the present work, the formulation was based on a pseudo-transient approach, which results in the same behavior as under-relaxed steady simulation without modifications in the original code (Versteeg and Malalasekera, 2007 and Maliska, 2004).

2.1. Gaseous-phase equations

The Favre-averaged equations of the low-Mach number, variable density flow are given as follow:

$$\frac{\partial \bar{\rho}}{\partial t} + \frac{\partial \bar{\rho}\widetilde{U_\iota}}{\partial x_i} = \overline{\overline{S_{mass}}} \tag{1}$$

$$\frac{\partial \bar{\rho}\widetilde{U_\iota}}{\partial t} + \frac{\partial \bar{\rho}\widetilde{U_\iota}\widetilde{U_J}}{\partial x_j} = -\frac{\partial \bar{p}}{\partial x_i} + \frac{\partial \tau_{ij}}{\partial x_j} + \bar{\rho} g_i + \overline{S_\iota} \tag{2}$$

$$\frac{\partial \bar{\rho}\tilde{f}}{\partial t} + \frac{\partial \bar{\rho}\tilde{f}\widetilde{U_J}}{\partial x_j} = + \frac{\partial}{\partial x_j}\left(\frac{\mu_t}{\sigma_f}\frac{\partial \tilde{f}}{\partial x_j}\right) + \overline{S_f} \tag{3}$$

$$\frac{\partial \bar{\rho}\widetilde{f''^2}}{\partial t} + \frac{\partial \bar{\rho}\widetilde{f''^2}\widetilde{U_J}}{\partial x_j} = + \frac{\partial}{\partial x_j}\left(\frac{\mu_t}{\sigma_f}\frac{\partial \widetilde{f''^2}}{\partial x_j}\right) + C_g\mu_t\left(\frac{\partial \tilde{f}}{\partial x_j}\right)^2 - C_D\frac{\bar{\rho}\varepsilon}{k}\widetilde{f''^2} \tag{4}$$

Where for the *k*-*ε* model:

$$\frac{\partial \bar{\rho}k}{\partial t} + \frac{\partial \bar{\rho}k\widetilde{U_J}}{\partial x_j} = + \frac{\partial}{\partial x_j}\left(\frac{\mu_t}{\sigma_k}\frac{\partial k}{\partial x_j}\right) + 2\mu_t\widetilde{S_{\iota J}}\cdot\widetilde{S_{\iota J}} - \rho\varepsilon \tag{5}$$

$$\frac{\partial \bar{\rho}\varepsilon}{\partial t} + \frac{\partial \bar{\rho}\varepsilon\widetilde{U_J}}{\partial x_j} = + \frac{\partial}{\partial x_j}\left(\frac{\mu_t}{\sigma_\varepsilon}\frac{\partial \varepsilon}{\partial x_j}\right) + C_{1\varepsilon}\frac{\varepsilon}{k}2\mu_t\widetilde{S_{\iota J}}\cdot\widetilde{S_{\iota J}} - C_{2\varepsilon}\rho\frac{\varepsilon^2}{k} \tag{6}$$

$$\mu_t = \bar{\rho}C_\mu\frac{k^2}{\varepsilon} \tag{7}$$

$$\tau_{ij} = \rho\widetilde{u_\iota' u_J'} = \frac{2}{3}\delta_{ij}\left(\bar{\rho}k + \mu_t\frac{\partial \widetilde{U_k}}{\partial x_k}\right) - \mu_t\widetilde{S_{\iota J}} \tag{8}$$

$$\widetilde{S_{\iota J}} = \frac{\partial \widetilde{U_\iota}}{\partial x_j} + \frac{\partial \widetilde{U_J}}{\partial x_i} \tag{9}$$

Where, $\bar{\rho}$ is the density of the gaseous mixture, g_i is the i component of the gravity acceleration, $\tilde{f}$ is the Favre mean value of mixture fraction, $\widetilde{U_i}$ is the velocity, μ_t is the turbulent viscosity, $\bar{p}$ is the pressure, $\widetilde{f''^2}$ is the Favre mean value of variance of the mixture fraction, σ_f is the turbulent Prandtl/Schmidt number for mixture fraction (which has the value of 0.85 in this work), k is the turbulent kinetic energy, ε is the dissipation of k, $\overline{S_x}$ are the source terms to account for inter-phase coupling of the physical quantity x, and δ_{ij} is the kronecker's delta operator. The five adjustable constants: C_μ, σ_k, σ_ε, $C_{1\varepsilon}$, $C_{2\varepsilon}$ have their standard values, respectively: 0.09, 1.00, 1.30, 1.44 and 1.92 as given by Versteeg and Malalasekera (2007) and Jones and Whitelaw (1982). The adjustable constants C_D and C_g defined in the Eq. (4) have respectively the values 2.00 and 2.86.

For the present study, the chemical reactions are modeled with the conventional β-PDF flamesheet model (Turns, 2000 and Versteeg and Malalasekera, 2007). In this model a global one-step infinitely fast chemical reaction is assumed and the intermediate reactions are ignored. This combustion model is based on the transport of the mixture fraction (Eq. (3)) and its variance (Eq. (4)) where a probability density function with presumed shape is defined to estimate the mean values of the properties related with the reaction model, which is necessary when modeling a turbulent flame (Versteeg and Malalasekera, 2007). The global one-step, infinitely fast, stoichiometric reaction of ethanol with air is used to define the chemical reactions in this work, which is given by:

$$C_2H_5OH + 3{,}00(O_2 + 3{,}76N_2) \rightarrow 2{,}00CO_2 + 3{,}00H_2O + 11{,}28N_2$$

The liquid droplets evaporate and the resulting fuel vapor mixes with the surrounding gas. Unlike a two-inlet pure gaseous system, the fuel in the above formulation is in the liquid form (Apte *et al.*, 2009). The fuel mass fraction comes from the mixture fraction, like the mass fractions of the other chemical species that compose the global reaction mechanism. Combustion takes place in the gaseous phase. Hence, the mass of fuel that evaporates of the droplets have to be transformed in mixture fraction with the Eq. (11).

The source terms in the gas-phase continuity, mixture-fraction, and momentum equations are obtained from the equations governing droplet dynamics (Eqs. (13), (14), (18), (20) and (24)). This source terms is used as the same formulation presented by Fluent (2006), which corresponds to a simplification. A more detailed formulation for this source terms, which also considers the influence of the disperse phase on turbulence is given by Chrigui *et al.* (2009). The expressions for source terms are:

$$\overline{\dot{S}_{mass}} = \sum \Delta m_P / (\Delta V \cdot \Delta t) \tag{10}$$

$$\overline{S_f} = \frac{s}{s + Y_{ox,0}} \overline{\dot{S}_{mass}} \tag{11}$$

$$\overline{S_i} = \sum \left(\frac{1}{\tau} (\boldsymbol{u} - \boldsymbol{u}_P) - \left(1 - \frac{\rho}{\rho_P}\right) \boldsymbol{g} \right) \frac{m_P}{\Delta V} \tag{12}$$

Where, Δm_P is the mass variation of a droplet when it pass throw a cell, ΔV is the volume of a cell, Δt is the integration time step of the gaseous phase, s is the ratio of the mass fractions of oxygen and fuel in a global stoichiometric proportion, $Y_{ox,0}$ is the mass fraction of oxigen at a point contains only oxidant, , τ is the relaxation time, $\boldsymbol{u}$ the gas-phase velocities interpolated to the droplet location, $\boldsymbol{u}_p$ denotes the droplet velocity, ρ_P and ρ are the droplet and gas-phase densities.

It is worthy to note that the mixture fraction is defined in a different form in this work as commonly defined in the combustion literature. The maximum value of mixture fraction corresponds to a cell fully of fuel, and not to the boundary condition of the fuel injector, as is commonly done in pure gaseous flows analysis. The definition used in this work was done by the fact that the mixture fraction in the gaseous phase comes from the evaporation of the droplets.

2.2. Liquid-phase equations

Droplet dynamics are simulated using the Separated Flow (SF) method (Faeth, 1983) with a Lagrangian point-particle model. This kind of formulation is valid in regions of dilute spray. Faeth (1983) define these regions when the droplets are spaced in a distance larger than two diameters. Unlike this definition Fluent (2006) defines the regions of dilute spray as the regions where the liquid phase has a volume fraction less than 10-12%. Observing the measurements made by Masri (2009), one can obtain the approximate value of 0.05% of volume fraction of the liquid phase already near the nozzle. This characteristic is due to the form of atomization and injection applied by Masri (2009).

To proceed with this approach it is assumed that (1) the density of the droplets is much greater than that of the carrier fluid, (2) the droplets are dispersed and collisions between them are negligible, (3) droplet deformation effects are small, and (4) motion due to shear is negligible (Apte *et al.*, 2009). Under these assumptions, the Lagrangian equations governing the droplet motions become (Fluent, 2006).

$$\frac{d\boldsymbol{x}_P}{\partial t} = \boldsymbol{u}_P \tag{13}$$

$$\frac{d\boldsymbol{u}_P}{\partial t} = \frac{1}{\tau}(\boldsymbol{u} - \boldsymbol{u}_P) - \left(1 - \frac{\rho}{\rho_P}\right)\boldsymbol{g} \tag{14}$$

$$\frac{1}{\tau} = \frac{18\mu}{\rho_P d_P^2}\frac{C_D Re}{24} \tag{15}$$

Here, $\boldsymbol{x}_P$ is the position of the droplet centroid, d_P is the droplet diameter, $\boldsymbol{g}$ is the gravitational acceleration, μ is the molecular viscosity of the gas surrounding the droplet, C_D is the drag coefficient and Re is the relative Reynolds number, defined as:

$$Re = \frac{\rho d_P |\boldsymbol{u} - \boldsymbol{u}_P|}{\mu} \tag{16}$$

$$C_D = \begin{cases} \frac{24}{Re}\left(1 + \frac{Re^{2/3}}{6}\right) : 0 < Re < 1000 \\ 0.44 : \qquad Re \geq 1000 \end{cases} \tag{17}$$

The above correlation for drag coefficient is given by Yuen and Chen (1976).

The droplet evaporation is modeled based on a two-stage model for an isolated droplet (Faeth, 1983 and Fluent, 2006). The process of mass transfer of the droplet is divided in two stages: in the first the rate of mass transfer is driven by the difference in fuel vapor concentration between the surface of the droplet and its local surroundings, in the second stage the rate is driven by the difference of the temperature, also between the surface of the droplet and its local surroundings. The change of stages takes place when the droplet reaches its boiling point at the environment conditions. Also in the second stage the temperature of the droplet is constant, and all the heat the droplet receives becomes latent heat of vaporization.

Droplet heating is modeled by the infinite-liquid-conductivity model (Sirignano, 2010), in which there is a spatially uniform but time-varying droplet temperature. Only in the first stage of the evaporation process the heat the droplet receives increases its temperature. The evaporation model is a heat and mass transfers coupled phenomena but here they are decoupled to simplify the computations.

The Lagrangian equations governing droplet temperature and mass for the first stage become:

$$m_p c_p \frac{dT_p}{dt} = hA_p\left(T_\infty - T_p\right) \tag{18}$$

Here, the heat transfer coefficient h is evaluated based on the correlation proposed by Ranz and Marshall (Fluent, 2006):

$$Nu = \frac{hd_p}{k_\infty} = 2.0 + 0.6\,\mathrm{Re}_d^{1/2}\,\mathrm{Pr}^{1/3} \tag{19}$$

For this stage the mass transfer is given by:

$$\frac{dm_p}{dt} = -N_l A_p M_{w,l} \tag{20}$$

$$N_L = k_C\left(C_{L,s} - C_{L,\infty}\right) \tag{21}$$

$$C_{L,s} = \frac{p_{sat}\left(T_p\right)}{T_p R} \text{ and } C_{L,\infty} = X_L \frac{p}{T_\infty R} \tag{22}$$

$$Sh_{AB} = \frac{k_C d_p}{D_{L,m}} = 2.0 + 0.6\,\mathrm{Re}_d^{1/2}\,Sc^{1/3} \tag{23}$$

Where, m_P is the mass of the droplet, c_P is the specific sensible heat of the liquid, T_P is the temperature of the droplet, T_∞ is the temperature of the gaseous phase, A_P is the surface area of the droplet, k_∞ is the thermal conductivity

of the gaseous phase, Pr is the Prandtl number, $M_{w,L}$ is the molecular weight of the liquid, k_C is the mass transfer coefficient, $C_{L,S}$ is the concentration of liquid vapor on surface of the droplet, $C_{L,\infty}$ is the concentration of liquid vapor on gaseous phase, p_{sat} is the saturation pressure of the liquid, X_L is the mole fraction of the liquid vapour, p is the gaseous pressure, R is the universal constant of ideal gases, $D_{L,m}$ is the binary mass diffusion coefficient of vapour of the liquid in air and Sc is the Schmidt number.

The second stage equations are:

$$\frac{dd_P}{dt} = \frac{2}{h_{fg}\rho_P}\left[\frac{Nu \cdot k_\infty}{d_P}(T_\infty - T_P)\right] \tag{24}$$

$$Nu = \frac{ln(1+B)}{B}\left(1 + 0.39Pr^{1/3}Re^{1/2}\right),\ B = \frac{c_P}{h_{fg}}(T_\infty - T_P) \tag{25}$$

Here, h_{fg} is the enthalpy of vaporization,

2.3. Turbulent dispersion of droplets

When a turbulent flow is modeled with a RANS turbulence model, special care should to be taken to reproduce the turbulent dispersion of droplets. Neglecting dispersion implies that drops follow deterministic trajectories prescribed by their initial condition at the injector exit and mean gas properties throughout the flow field (Faeth, 1983).

To reproduce the turbulent dispersion of droplets in this work, a combination of models presented by Faeth (1983) and by Fluent (2006) was used. The analysis made by Faeth (1983) indicates stochastic methods as a good alternative to reproduce this kind of dispersion. Stochastic methods involve particle dispersion directly.

In this work, the instantaneous gas velocity replaces the mean velocity in the governing equations of droplets. As droplet pass through the flow, it is assumed to interact with individual eddies. During this interaction the flow properties are assumed to be constant. Thus, each interaction deflects the droplet trajectory as dictated by the instantaneous eddy velocity.

The mean gas velocity and the turbulent kinetic energy compound the instantaneous gas velocity over the droplets. The turbulence is considered isotropic with components having a Gaussian distribution for this computation. The standard deviation of the distribution is taken to be $\sqrt{2k/3}$. Thereby, to obtain the instantaneous velocity over the droplet the distribution is randomly sampled when a particle enters an eddy to obtain the instantaneous velocity as $\widetilde{\boldsymbol{u}} = \widetilde{\mathbf{U}} + \widetilde{\mathbf{u}}'$.

This model employs the interaction time by the same manner as Fluent (2006) and Faeth (1983), where the droplet is assumed to interact with the gaseous phase over the smallest eddy lifetime and eddy crossing time. When the interaction time is over, a new value of the instantaneous velocity is computed. The lifetime and crossing time are defined by:

$$t_e = -\frac{L_e}{\sqrt{2k/3}}log(r) \tag{26}$$

$$t_{cross} = -\tau ln\left(\frac{1-L_e}{\tau|\boldsymbol{u}-\boldsymbol{u}_P|}\right) \tag{27}$$

$$L_e = C_\mu^{3/4}\frac{k^{3/2}}{\varepsilon} \tag{28}$$

Where, t_e is the eddy lifetime, t_{cross} is the eddy crossing time and r is a uniform random number between 0 and 1.

3. NUMERICAL METHOD

The code used in this work was developed originally for LES by Fukumasu (2010), which also validated its operation, changes were done to implement the k-ε Standard turbulence model. This code was based on a finite-volume method to solve the low-Mach number, variable density gas-phase flow equations on cartesian grids with the co-located scheme. In this co-located scheme, the velocity and pressure fields are stored and solved at the centroids of the control volumes.

3.1. Gaseous-phase equations

The velocity and pressure fields are coupled by the Pressure Implicit and Momentum Explicit (PRIME) scheme (Maliska, 2004). The scalar fields (k, ε and mixture fraction) and the dispersed field are advanced after the computation of the velocity field.

A first-order upwind scheme is used for advective terms and centered differencing for the diffusive terms. Once the simulation is pseudo-transient, all terms, except the inter-phase source terms, are treated implicitly using first order Euler method for temporal discretization.

After the mixture fraction field is computed, the density and temperature fields are obtained from the β-PDF flamesheet model. The algorithm employed here to solve all the transport equations is given by the steps bellow:

- Compute the velocity and pressure fields using the PRIME algorithm. The density field and the turbulent viscosity are available at previous time level.
- Solve the k and ε equations to calculate the turbulent viscosity, used in the velocity next step.
- Solve the transport equation for the mixture fraction and compute the new field of density and temperature.
- Compute the disperse phase.
- If the solution is not converged, the time is advanced and the procedure restarts by the first step.

Versteeg and Malalasekera (2007) mention the steady state calculations may be interpreted as pseudo-transient solutions with spatially varying time steps. These authors compare an under-relaxed steady state equation to an implicit transient equation and achieve a relation between the time step and the under-relaxation coefficient for the steady-state solution. Fluent (2006) mentions the under-relaxation of steady-state equations, also known as implicit relaxation, is used in the pressure-based solver to stabilize the convergence behavior of the outer nonlinear iterations by introducing selective amounts of the physical quantity in the system of discretized equations. Then it is defined a Courant-Friedrichs-Lewy number (CFL), which is used in this work.

$$CFL = \frac{\alpha}{1-\alpha} \tag{29}$$

Where α is the under-relaxation coefficient for the steady-state equation. Thus, the time step is defined by:

$$\Delta t = min\left(CFL\frac{\rho_i \Delta V}{A_i}\right) \tag{30}$$

Here, ρ_i is the density in the i^{th} cell, and A_i is the coefficient related of cell i of the main diagonal of the linear system used to solve the discretized momentum equations. With the CFL number defined in this work the resulting time step is approximate 1.5×10^{-5} during the calculations.

3.2. Droplet equations

The droplet equations are advanced using the implicit first order Euler scheme. Apte *et al.* (2009) define that the sub-cycling of the droplet equations becomes necessary. They use a comparison among the time scales of droplet transport equations and the time step of the flow field to define the time step for droplet equation advancement the minimum of these time scales and time step. This choice of calculating the time steps for the computing of the discrete phase is acceptable when the time steps of the gaseous phase are short. Thus, for Apte *et al.* (2009) this is not a problem when using a turbulence model like LES that requires a short time step. But when using RANS this choice can turn the computing process very slow. It is important to note here the spray calculated is represented by the transport of individual droplets in the computational domain.

Therefore, in this work it was used the same scheme given by Fluent (2006), which a step length factor is defined. This factor specify how many times the equations of a particular droplet will be calculated when it passes through a cell. With this calculation scheme the time steps are bigger avoiding a slow computation.

3.3. Particle Tracking

On the calculation of droplets, at each sub-cycle, their positions have to be known to enable the program to interpolate the gaseous phase quantities in these positions. In this work each droplet is calculated individually and the number of these particles is the order of a million, thus locate each particle at each sub-cycle have to be done fast to avoid high computational cost. As Apte *et al.* (2009) mentions in their work, solving the Lagrangian equations thus requires addressing the following key issues: (i) efficient search for locations of droplets, and (ii) interpolation of gas-phase properties to the droplet location.

The Particle Tracking can be divided in two steps: verification if droplets are into a cell and searching them into the calculation domain.

The criterion used in the verification step follows the same used by Apte *et al.* (2003). In this criterion, vectors (***ppv*** –particle-projection vector) are created between the particle position and its projection on each face of the cell in which the verification is applied. These vectors are compared with the respective outward face-normals vectors (***fnv***) of the cell. When the particle is within the control volume, these ***ppv's*** point the same way as the ***fnv's***, and when the particle is not within the cell, the vectors do not point same way.

An approach of successive neighbor search described by Li and Modest (2001) is used to select the cell to which the verification should be applied. This approach, as in the verification, uses a comparison between vectors to select the next cell to search the particle. One vector (***cpv*** – centroid-particle position vector) created between the centroid of the last cell where the verification was applied and the position of the particle is compared with the vectors (***ccv*** – centroid-centroid vectors) defined by the last cell centroid and its neighbor cells centroids. The ***ccv*** that better approximates to the ***cpv*** will indicate the next cell where the criterion will be applied, which is the neighbor cell that composes the ***ccv***.

As Apte *et al.* (2003) organized their search algorithm, in this work, when the successive search algorithm fails a modified brute-force scheme is recovered. The modified brute-force approach, as denominated by Lohner (2005), applies the verification over the last cell of the mesh in which the successive search algorithm stops. If the particle is not encountered, this algorithm starts to search the particle over the elements surrounding that cell and goes in this way until all the elements of the mesh are verified.

4. PHYSICAL MODEL

The experimental data used in this work, was extracted from the work of Masri (2009). This work reports measurements of mean temperature, axial velocity, turbulence and droplets fields in pilot-stabilized jet flames of dilute sprays where acetone or ethanol is used as liquid fuel.

Figure 1 presents a schematic of the piloted spray burner setup used by Masri (2009). The central nozzle is 10.5mm ID and shrouded with a perforated annular pilot flame. The central jet is stabilized by the shroud of combustion products that exits the annulus. A 104 mm diameter co-flow surrounds the burner with a uniform velocity of 4.5m/s with low turbulence intensity. The entire burner assembly is mounted inside a 29 x 29 cm vertical wind tunnel which supplies filtered co-flowing air stream at 4.5 m/s with low turbulence intensity. An ultra-sonic atomizer is positioned 215 mm upstream of the nozzle exit plane providing droplets with zero initial momentum and a Sauter Mean Diameter of 40 microns. The resulting droplets are carried by a co-flowing air to the exit plane where velocity and droplet distribution are measured, providing a set of boundary conditions. Masri (2009) mentions some evaporation takes place between the atomizer and the nozzle exit plane leading to an overall cooling of the stream. Despite the amount of liquid fuel measured was 0.0375 kg/min the atomizer was fed with 0.045 kg/min.

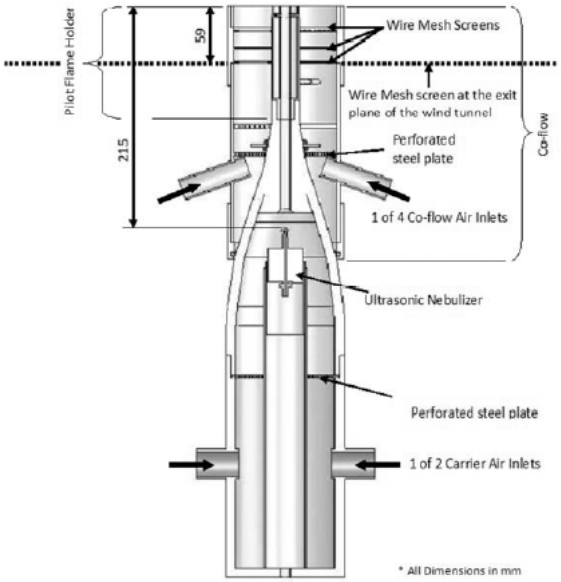

Figure 1. Burner schematic setup, Masri (2009)

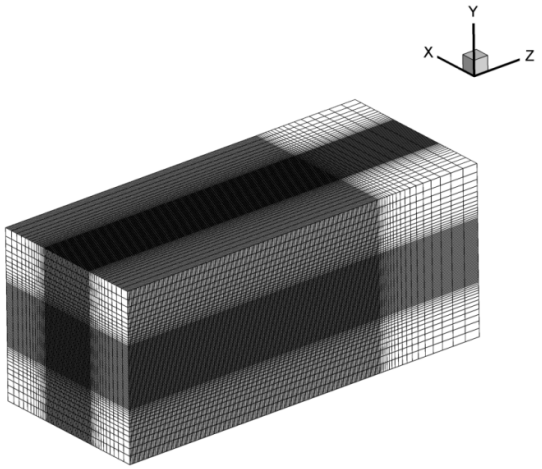

Figure 2. Isometric view of the computational grid

4.1. Grid and boundary conditions

Figure 2 shows the grid used in the numerical simulations. The domain size had dimensions of 42*D* x 42*D* x 100*D* with *D* being the diameter of the fuel nozzle. The cartesian grid has a size of 2,421,900 cells that composed by 90 x 90 x 299 grid nodes in the *x*, *y* and *z* directions, respectively. For the first 70*D* in the axial direction (*z*) the grid is equidistant; downstream of that zone, the grid points are linearly expanded with an expansion ratio of 1.15. In the *x* and *y* directions, the grid points are uniform spaced for 7.75*D* from the center line of the jet to its boundaries, and the adjacent space was completed with a linearly expansion ratio of 1.15.

The inflow conditions for velocity were of Dirichlet type and linearly interpolated onto the grid from the measured profiles of velocity. For the other physical quantities, in except for pressure, the boundary conditions are also of Dirichlet type. Especifically, for mixture fraction in all the extension of injection face the value null, set up (due to this property comes from the evaporation of the droplets). The k and ε were obtained by the Eq. (31) and Eq. (32) respectively. Figure 8 presents the values of experimental data that are used as boundary conditions for axial velocity and its fluctuations. Pressure boundary condition in the injection face was not prescribed, because in the PRIME scheme the values of velocities that are boundary conditions do not need to be corrected, thus the pressure gradient in faces are null. On the other faces that delimits the computational domain the boundary conditions was defined as a constant pressure outlet, with the pressure like Dirichlet type with null value, and the other quantities as Neumann type with null value.

$$k = \sqrt{u'_i u'_i / 2} \tag{31}$$

$$\varepsilon = C_\mu^{3/4} \, k^{3/2} / 0.07L \tag{32}$$

Where: u'_i is the RMS of the fluctuation of the velocity linearly interpolated onto the grid from the measured profiles, and L is the turbulent integral scale defined as the radius of the nozzle diameter. It is believed that the presence of any confinement, as wind tunnel walls, did not exert any notable influence on the results.

The boundary conditions for droplets are taken directly from experimental measurements. Once achieved the droplet distribution curves, it was used a random launcher for them. The stochastic droplet launcher is programmed to randomly launch these quantities, one by one, in space using polar coordinates (defining an angle and a radius to launch). First, the launcher selects an angle and after a radius following a distribution curve of liquid mass launched per radius. Second, the particle to be launched is extracted by another random function from a distribution curve of number of particles by droplet diameters. Once defined the diameter of the droplet a joint relation between particles diameter and velocity is used to define the launch velocity of the droplet. With this scheme almost a thousand particles are launched per time step.

5. RESULTS AND DISCUSSION

The results were collected when the solution was considered converged, which means almost 30,000 iterations. The convergence was determined when the results did not presented significant change with iterations advancement.

OpenMP™ parallel processing method was applied to the solver, improving computation speed. The overall computational time was less than 120 CPU-hours on a SGI® Altix® XE320 with 16 processors.

Figure 3 and Figure 4 present respectively the radial profile of the axial velocity in a distance of 10*D* and 20*D* from the nozzle. The velocities are normalized with the centerline jet exit velocity U_o. The continuous line represents the results of the simulations and the dashed line corresponds to the experimental data.

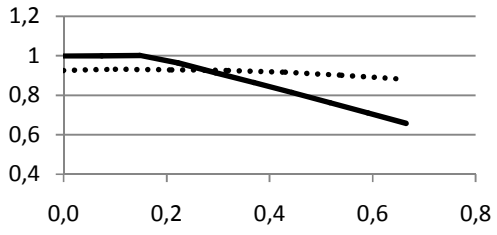

Figure 3. Normalized axial velocity *U/Uo* at the plane *z/D* 10

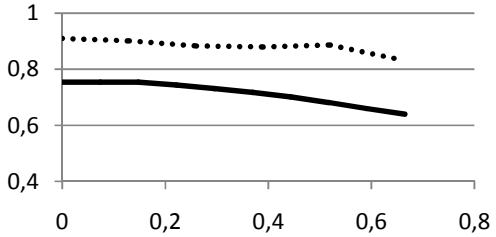

Figure 4. Normalized axial velocity U/U_o at the plane z/D = 20

It can be seen the simulated velocities decay in the axial direction faster than the velocities of the experimental data. Analyzing the radial profile, Fig. 3, it can be noted the radial transport of axial momentum in the simulation is less than in the experiments. From these results, one can conclude that in the simulations the diffusive transport of momentum is over predicted. One reason of the discrepancies observed can be attributed to the problems related with the modeling of the combustion process that were strongly coupled with momentum transport.

Figure 5, Figure 6 and Figure 7 present the radial profile of the temperature in the distances of 10*D*, 20*D* and 30*D* from the nozzle. Figure 5 presents higher temperatures near the centerline of the jet in the simulations than in the experiment. This discrepancy is due to the lower diffusive transport of mixture fraction in the radial direction. The radial temperature profiles (Figs. 5 to 7) indicate that the flame spreads radially slower in the simulation than in the experiment.

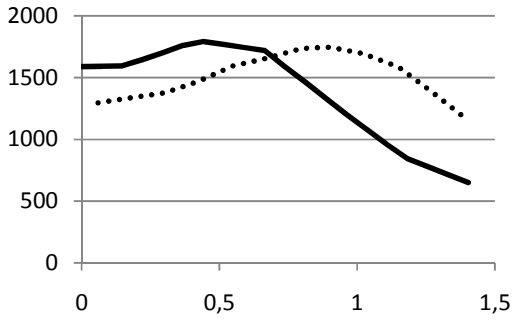

Figure 5. Temperature in K per *r* in *z/D* 10

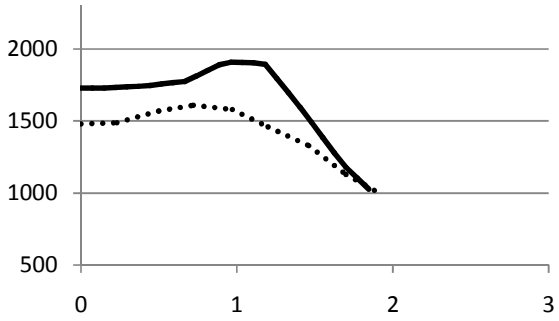

Figure 6. Temperature in K per *r* in *z/D* 20

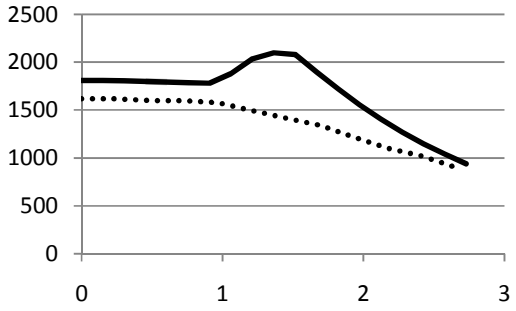

Figure 7. Temperature in K per *r* in *z/D* 30

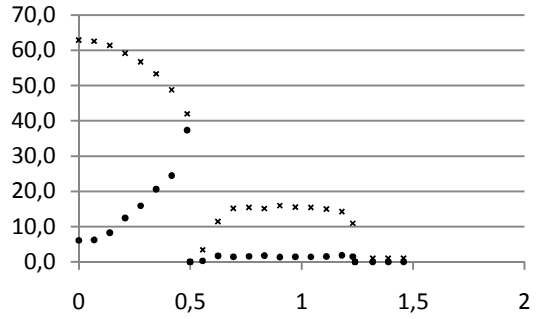

Figure 8. Boundary conditions for axial velocity (x) and its turbulent fluctuations (●) in m/s

The negligence of the evaporative cooling could be one of the responsible facts for the discrepancies observed. The representation of this phenomenon would reduce the temperature of the gas phase, which could reduce the peak of temperatures observed in the simulations. Another issue are the limitations in the global chemistry mechanism used in this work. In the combustion model used here (β-PDF flamesheet), the one-step, infinitely fast global reaction mechanism considers that when the mixture is in stoichiometric ratio the reagents will completely react to generate the products. In this case, when there is the stoichiometric mixture, the temperature of the gas mixture is the same of the adiabatic ethanol flame temperature. Thus, observing the experimental data, it can be noted that this temperature is not reached. This behavior can be explained by the fact that the experimental flame did not react in an adiabatic environment and not necessarily in a stoichiometric mixture or even in an equilibrium reaction as was considered in the combustion model used in the simulations.

Eventually the evaporation process could also be responsible for these discrepancies observed. As noted by Rochaya (2007), the incorrect modeling of this phenomenon could change considerably the temperature field. With the flamesheet model, when droplets evaporate hardly in the core of the spray, high values of mixture fraction are achieved in this region. If the values of mixture fraction in this region are higher than the value of stoichiometric mixture fraction, when this quantity spreads radially, at some place, the mixture will reaches the stoichiometric proportion achieving temperatures close to the adiabatic flame temperature. Because of this behavior, it will always produce the peacks of temperature in the gaseous flow. However, if the droplets evaporate with a lower rate in the core region, achieving lower values of mixture fraction than the stoichiometric value, the high temperatures will be avoided reducing these discrepancies in the temperature field. One way to evaluate the evaporation rates is by making comparisons between numerical and experimental droplets size distributions, which is not done yet in this study.

6. SUMMARY AND CONCLUSIONS

In this work a k-ε Standard simulation of a spray flame in an open air combustor under the conditions corresponding to an experiment by Masri (2009) was performed. An Eulerian–Lagrangian formulation was applied to calculate the development of the reactive spray. The variable density, low-Mach number equations for reacting turbulent flows with phase change due to droplet evaporation are solved on a tridimensional Cartesian mesh. The droplet dynamics was modeled using the point-particle approach and an infinite-liquid-conductivity model for evaporation.

The droplet evaporation was calculated by a two-stage approach which is primarily governed by mass-diffusion and after by heat transfer. In the first stage the vapor mass-fractions in the surrounding fluid are considerably lower than those at the droplet surface and droplet temperature is less than ethanol boiling point. Already in the second stage, the

temperature of the droplet is higher than the temperature of ethanol boiling point, so than the evaporation is controlled by heat transfer. The influence of droplet evaporation on mixture fraction dissipation rates was pronounced.

The computed gas-phase temperature and velocity present some discrepancies when compared with the experimental data. The main reasons of these discrepancies were linked to the combustion model and to the absence of the evaporative cooling. Investigations of droplets distribution and evaporation model can give a more complete diagnostics of the problems observed in this spray flame model. Hence, future work will include the refinement of the computational methods with regard to droplet evaporation approaches.

7. ACKNOWLEDGEMENTS

The authors would like to thank the Coordenação de Aperfeiçoamento de Pessoal de Nível Superior (CAPES) for supporting of this work under the grant ‘‘CAPES-PRÓ-ENGENHARIAS / ESTUDO COMPUTACIONAL E EXPERIMENTAL DE CHAMAS TURBULENTAS DE ETANOL’’- PE004/2008.

8. REFERENCES

Apte, S. V., Mahesh, K. and Moin, P., 2009, “Large-eddy simulation of a evaporating spray in a coaxial combustor”, Proceedings of the Combustion Institute, Vol.32, pp. 2247-2256.

Apte, S. V., Mahesh, K., Moin, P., Oefelein, J. C., 2003, “Large-eddy simulation of swirling particle-laden flows in a coaxial-jet combustor”, International Journal of Multiphase Flows, Vol.29, pp. 1311-1331.

Chrigui, M., J., Hage, M., Dreizler, Sadiki, A., Janicka, A., 2009, “Experimental and Numerical Analysis of Spray Dispersion and Evaporation in a Combustion Chamber”, Atomization and Sprays, Vol.19, pp. 929-955.

Düwel, I., Ge, H.-W., Kronemayer, H., Dibble, R. Gutheil, E., Schulz, C., Wolfrum, J., 2007, “Experimental and numerical characterization of a turbulent spray flame”, Proceedings of the Combustion Institute, Vol.31, pp. 2247-2255.

Faeth, G. M., 1983, “ Evaporation and combustion of sprays”, Prog. Energy Combust. Sci., Vol.9, pp. 1-76.

Fluent, 2006, “User’s Guide”. User’s guide of the software Fluent version 6.3.26.

Fukumasu, N. K., 2010, “Modelagem de uma chama de difusão turbulenta pela simulação das grandes escalas”, MSc. Thesis, University of São Paulo, São Paulo, Brazil, 119p.

Jones, W. P. and Whitelaw, J. H., 1982, “Calculation of Turbulent Reacting Flows: A Review”, Combustion and Flame, Vol. 48, pp. 1-26.

Kuo, K. K., 1986, “Principles of Combustion”, John Wiley & Sons, Inc., United States of America, 810p.

Li, G., Modest, M. F., 2001, “An Effective Particle Tracing Scheme on Strucutured/Unstrucutured Grids in Hybrid Finite Volume/PDF Monte Carlo Methods”, Journal of Computational Physics, Vol.173, pp. 187-207.

Lohner, R., 1995, “Robust, Vectorized Search Algorithms for Interpolation on Unstructured Grids” , Journal of Computational Physics, Vol.118, pp. 380-387.

Maliska, C. R., 2004, “Transferência de calor e mecânica dos fluidos computacional”, Livros Técnicos Científicos Editora, Rio de Janeiro, Brazil, 453p.

Marinov, N. M., 1999, “ A Detailed Chemical Kinectics Mechanism for Hight Temperature Ethanol Oxidation”, Journal of Chemical Kinectics, Vol.31, pp. 183-220.

Masri, A. R., Gounder, J. D., 2009, “Turbulent Spray Flames of Acetone and Ethanol Fuels Aproaching Extintion”. Proceedings of Sixth Mediterranean Combustion Symposium.

Rochaya, D., 2007, “Numerical Simulation of Spray Combustion using Bio-mass Derived Liquid Fuels”, PhD. Thesis, Cranfield University, England, 292p.

Sirignano, W. A., 2010, “Fluid Dynamics and Transport of Droplets and Sprays”, Cambridge University Press, New York, United States of America, 462p.

Turns, S. R., 2000, “An introduction to combustion: concepts and applications”, McGraw-Hill series in mechanical engineering, Singapore, 676p.

Versteeg, H. K. and Malalasekera, W., 2007, “An Introduction to Computational Fluid Dynamics: The Finite Volume Method”, Pearson Education Limited, Harlow, England, 503p.

Yuen, M. C., Chen, L. W., 1976, “On Drag of Evaporating Liquid Droplets”, Combustion Science and Technology, Vol.14, pp. 147-154.

9. RESPONSIBILITY NOTICE

The authors are the only responsible for the printed material included in this paper.